Short title: High-resolution 4D spatiotemporal analysis of maize roots

Corresponding author:
Christopher N. Topp
Donald Danforth Plant Science Center
975 North Warson Road
St. Louis, MO 63132
Phone: (314) 587-1401
e-mail: ctopp@danforthcenter.org

High-resolution 4D spatiotemporal analysis reveals the contributions of local growth dynamics to contrasting maize root system architectures

Ni Jiang[1], Eric Floro[1], Adam L. Bray[1,2], Benjamin Laws[1],
Christopher N. Topp[1,§]

[1]Donald Danforth Plant Science Center, St. Louis, MO 63132 USA
[2]Division of Plant Sciences, University of Missouri-Columbia, 65211 USA
[§]Corresponding author

Author contributions: NJ, AB, EF and CNT conceived and designed research; NJ carried out analysis and developed novel tools; NJ, AB, EF, and BL collected data; CNT oversaw research; NJ and CNT wrote the paper.

ABSTRACT

Root systems are branched networks that develop from three simple growth properties of individual roots: elongation, curvature, and branching. Yet a mature maize root system has tens of thousands of roots that each interact with soil particles, water and nutrient patches, and microbial ecologies in the micro-environments surrounding each root tip. Although the plasticity of root growth to these and other environmental factors is well known, how these local processes contribute over time to global features of root system architecture is hardly understood. Here we employ an automated 3D root imaging pipeline to capture the growth of maize roots at four hour windows through seven days of seedling development. We model the contrasting architectures of two maize inbred genotypes and their hybrid to derive key parameters that distinguish complex growth patterns as a function of time. In aggregate, the local root growth patterns clearly contribute to the whole, despite a high degree of heterogeneity for individual root growth. We computationally extract a primary root from each root system and explore how differences in the radial and longitudinal developmental patterning along this axis contribute to the contrasting two root architectures. X-ray Computed Tomography analysis of mature field-grown root crowns verified that seedling growth trajectories persisted throughout development, and thus have a strong developmental genetic influence. The work connects the local and global scales of root system growth dynamics, providing the means for a function-valued approach to understanding the genetic and genetic x environment conditioning of root growth, and ultimately will link molecular processes at each root tip with global architecture patterns.

INTRODUCTION

Root system architecture (RSA) is very important for plant growth and productivity (Lynch, 1995). It affects water and nutrient acquisition efficiency (Doussan et al., 1998; Lambers et al., 2006), and changes in response to different environments (Hodge et al., 2009; Bao et al., 2014). A major goal for crop improvement is to understand the genetic basis of root system architecture (de Dorlodot et al., 2007; Topp et al., 2016). The genetic studies of shoot biomass have benefited from the quantification of plant growth at different time points (Muraya et al., 2017; Zhang et al., 2017). However, spatial and temporal aspects of root system architecture remain obscure.

Image-based phenotyping technologies enable high-throughput and non-destructive measurement of plant traits. In order to analyze root system architecture, a variety of root phenotyping systems have been developed. Minirhizotron tubes have been used to measure roots in the field at multiple time intervals (Johnson et al., 2001), but have the limitation of only examining the roots growing along the transparent tube. Nagel et al., 2012 developed GROWSCREEN-Rhizo where soil-filled rhizotrons are used to image visible roots though transparent plates. To analyze whole root systems in 3D, platforms where roots grow in gel cylinders have also been developed (Fang et al., 2009; Iyer-Pascuzzi et al., 2010; Clark et al., 2011; Zurek et al., 2015). X-ray computed tomography (Mooney et al., 2012a; Mairhofer et al., 2012), magnetic resonance imaging (Borisjuk et al., 2012; Metzner et al., 2015), and positron emission tomography (Jahnke et al., 2009; Garbout et al., 2012; Mathews et al., 2014), provide 3D quantification of root architecture in soil. Time-lapse imaging allows the dynamics of root growth and environmental responses to be studied (Iijima et al., 1998; Walter et al., 2002; Miller et al., 2007; French et al., 2009; Yazdanbakhsh and Fisahn, 2009; Lobet et al., 2011; Moore et al., 2013a; Rellán-Álvarez et al., 2015), however, these studies have been limited to root architecture analysis in 2D. Manually repeating 3D acquisitions at different time points enables the study of root growth in 3D (Fang et al., 2009; Clark et al., 2011; Topp et al., 2013; Symonova et al., 2015; van Dusschoten et al., 2016a), but at intervals of days, and with only global descriptions of the root architecture. Thus, the potential of automation and computer vision to link the local root growth processes to global architectural patterns has not been fully realized.

In this paper, we have developed an optical imaging system that allows frequent 3D monitoring of root growth. Using automatic time lapse imaging, growing root systems of B73, Mo17, and their hybrid were monitored over one week of development until day 11 after germination. Using computer vision, we computed the time function for each root, and analyzed the growth patterns in 3D space. Mathematical modelling of the time series revealed the key parameters that drive genotype-specific differences in root architecture, including timing of a sharp inflection point in relative growth rate. Our high-resolution spatiotemporal imaging and analysis approach will facilitate the study of growth responses to resource patches, other roots, soil particles, or other

heterogeneously distributed soil parameters at both the local and global level. This work will enhance the development of empirically-driven, probability-based growth models that can accurately predict root growth and root-environment interactions as a function of genotype.

RESULTS

Plant roots have typically been studied either individually in great detail, or globally as systems, but rarely both, especially as freely-growing 3D structures. In order to understand how local root growth patterns contribute to global architectures along both a real-time and a developmental time axis, we established a 4D analysis pipeline (Figure 1). We automated a 3D gel-based optical imaging system (Zurek et al., 2015; Topp et al., 2013) for time lapse, and paired it with DynamicRoots software (Symonova et al., 2015), and custom R code (available on Github: https://github.com/Topp-Roots-Lab/timeseries_analysis) to get the dynamic traits of individual branches based on the time series of 3D shapes. Two historically agronomically important maize inbred genotypes with contrasting root architectures, B73 and Mo17, and their hybrid were imaged every 4 hours across 8 days of development (164 hours total), from day 4 to day 11 after germination. The plants typically had only a primary root and one or two seminal roots at the beginning of the experiments, but over one hundred root branches by the end, including nodal and crown roots (SupplementaryMovie1), providing a wide spectrum of architectural complexity.

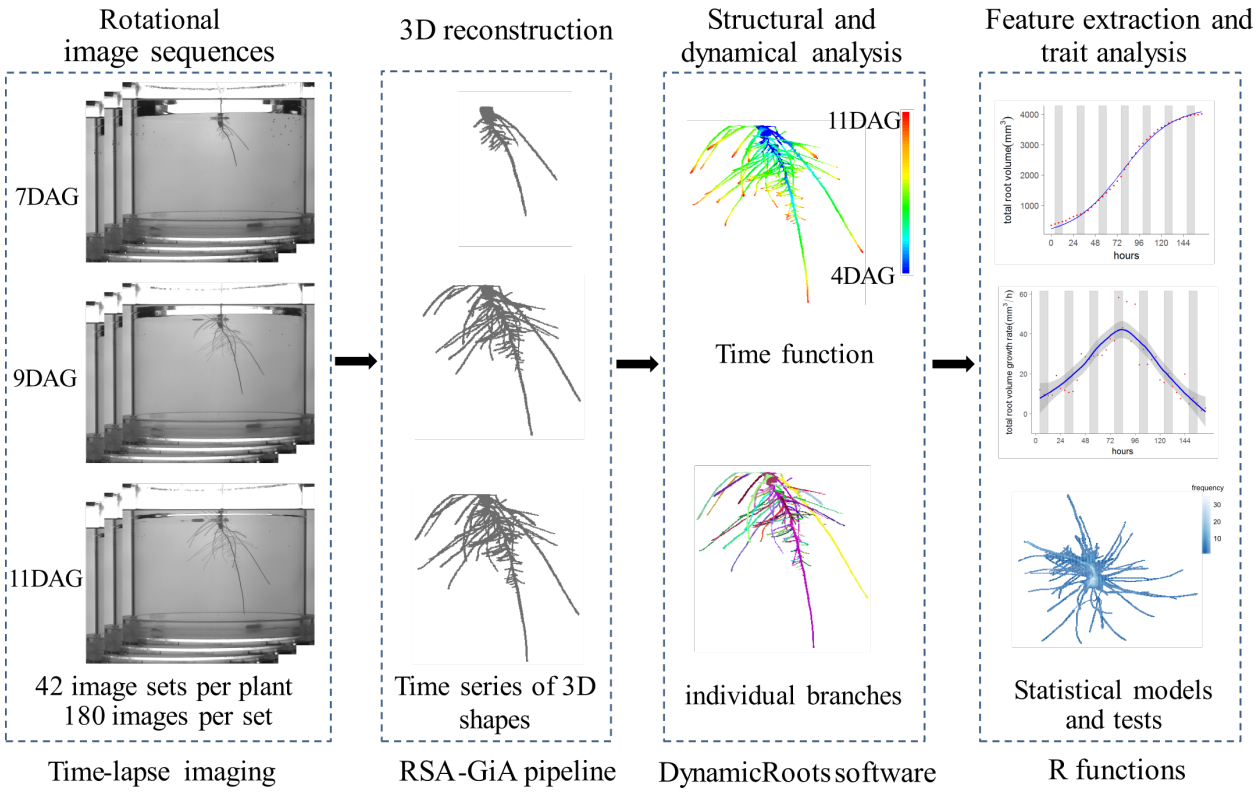

Figure. 1 Workflow for 4D analysis of maize roots. Rotational image sequences from our automatic 3D time lapse imaging system were imported and processed to reconstruct 3D models using the RSA-GiA pipeline. The reconstructed time series of 3D models were processed using DynamicRoots software. The phenotypic features were extracted and analyzed using custom R code (see Methods).

Quantifying global root traits at fine temporal scales reveals fundamental differences in growth patterns between two maize inbred genotypes and their hybrid

Phenotypic analysis of root architecture in a panel of diverse maize inbred lines has shown complex genotype-specific patterns that change during early development (Zurek et al., 2015), but their integration over time and the underlying cause is not yet understood. Using the automated imaging system, we were able to observe global-scale growth patterns on a highly resolved temporal scale. To provide information about the size and shape of the root systems, we compared total root volumes, lengths, and numbers, which all increase over time (Figure 2). Despite a highly controlled and homogeneous environment, the dynamic range of growth varied extensively within an individual plant as evidenced by the large spread of data. Yet phenotypic separation of the two genotypes could be identified very early in the experiment along the values of the mean curve (Figure 2a-c; t-tests for each time point in Table S1-S3). The hybrid values had the greatest intragenic variation, but the average values were largely intermediate, providing no evidence for heterosis in seedling root growth, similar to previous findings (Hund et al., 2012). While the total root volume and number of roots in B73 samples were consistently greater than Mo17 at all time points, initial differences in total root length disappeared by day 11 (Figure 2, Table S2). Since dry root weights from day 11 also showed that B73, Mo17 and their hybrid all had similar root biomass (Figure S1), we conclude that Mo17 and B73 fundamentally differ in how they allocate carbon resources for root foraging. B73 invests in relatively more, shorter, and "cheaper" roots (i.e. less biomass per unit of surface area), and Mo17 invests relatively more in the continued growth of extant roots, with their hybrid as intermediary. We investigated the duration of these trends by extracting identical 3D features from X-ray scanned root crown samples excavated from the field at flowering over two consecutive years. The phenotypic trends are remarkably consistent between B73 and Mo17, although the hybrids are much larger than either parent by this time (Figure S2). Our results suggest that a strong and persistent genetic influence on root carbon allocation investments can be detected at the seedling stage given sufficiently high-quality data.

To capture the underlying dynamics of these temporal relationships, we computed the rates of change (or velocities, the first derivative) and accelerations (changes in velocity, the second derivative) for the three global traits (Figure 2d-f). A sharp demarcation occurs in both inbred genotypes that separates increasing and decreasing growth rates for root volume and length. However the inflection point is delayed in Mo17 relative to B73 (Figure 2d,e), and slightly earlier in the hybrid. This transition is coupled to the rate of new roots in B73 and the hybrid, but

not in Mo17 (Figure 2f), reinforcing evidence for a fundamentally different process for patterning root architecture between the two genotypes that appears semi-dominant in the hybrid.

Despite the clear trend over the 1-week time interval, accelerations or decelerations between any two 4-hour time intervals were generally smooth - no significant differences were found for rates of change in total root number for any genotype at this temporal resolution, and in only a single interval each in B73 and the hybrid for root volume. Rates of change for total root length were more variable in all genotypes, but not in a consistent pattern (Figures 2d-f; Table S4). Diurnal patterns of growth in plant leaves and shoots (Walter et al., 2009) are well established, but evidence in grasses suggests that their roots do not change elongation patterns along day/ night cycles (Iijima et al., 1998; Walter et al., 2002). We compared the growth rates during the 4 hours before dark to the growth rate during the next 4 hours in the dark for each genotype. All three genotypes had differences ($p < 0.05$) in day/ night growth rates at some time points, but not others (Table S4), providing no strong evidence of diurnal regulation, which reinforces previous studies. We found that growth rates were predominantly driven by developmental time, rather than diurnal real-time.

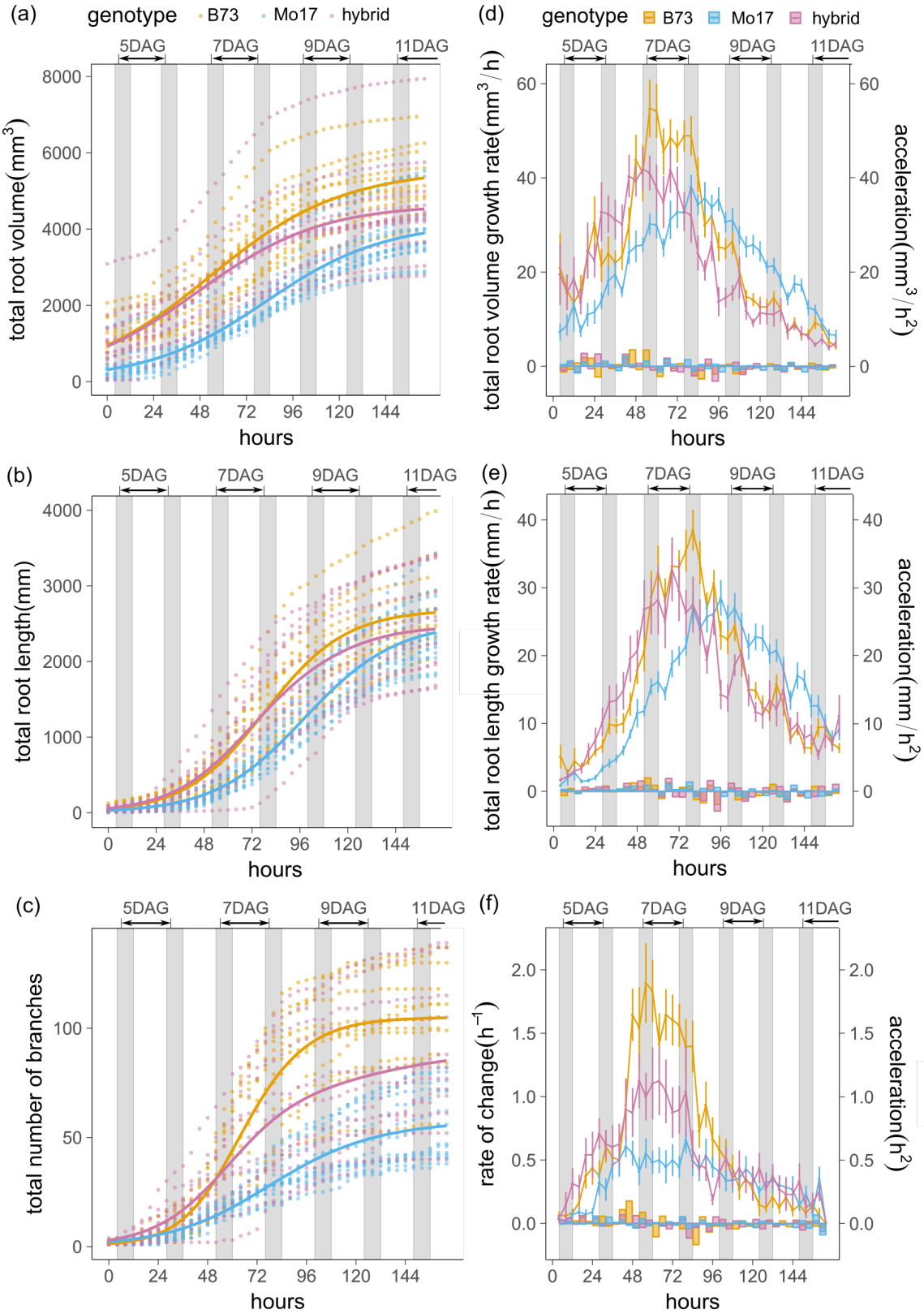

Figure 2. Global root traits dynamics revealing fundamental differences in growth pattern. Timecourse values of total root volume (a), total root length (b), and total root number (c). Each point represents an individual seedling, and the solid lines indicate mean values.

Timecourse of growth rates and accelerations of the total root volume (d), total root length (e), and total root number (f). Points represent the mean value of growth rates. Vertical error bars represent the standard errors. Barplots show the accelerations. The gray bars represented night time.

Modelling global growth patterns allows a direct comparison of key parameters that control more complex patterns

Non-linear models such as logistic growth functions can provide "function-valued" traits that integrate both real and developmental time to describe complex patterns of growth or architectural change (Barlow et al., 1991; Paine et al., 2012; Morris and Silk, 1992; Araya et al., 2016). After testing various nonlinear models for several fitting criteria (Table S5), we chose a 3-parameter logistic growth function to model the global trait dynamics (Figure 3; Methods). Parameter α_1 describes the "carrying capacity" of the function, which reports the maximum values of the modelled growth curve. B73 had significantly higher α_1 values for total root volume and total number of root branches, reflecting that B73 has a larger final volume and more branches than Mo17 (Figure 3). However, the α_1 values for total root length were not different, despite significantly larger values for B73 at each time point until hour 144. This result highlights the importance of capturing and integrating the time dimension through an appropriate model, rather than ad hoc analysis of individual time points, which may be misleading. Parameter α_2 represents the maximum rate of change and is a direct measure of the trends seen in Figures 2 d-f. It provides an explicit quantification of the different times at which the inflection point between increasing and decreasing growth trends were reached for a given trait. B73 and the hybrid begin slowing the rate at which root length and volume are added more than 24 hours prior to Mo17 (Figure 3a,b), although differences in the time at which additions of new lateral roots slowed were much less pronounced (Figure 3c). Parameter α_3 captures the slope of the growth curve, and except for total root volume, the values between B73 and Mo17 were significantly different, reflecting that the total number of branches and to a lesser extent total root length increased more sharply for B73. The overall growth trends for the hybrid were most similar to B73, although we note that range of values was typically larger than either parent (reflected in the long axes of the violin plots, Figure 3), suggesting the hybrid is less rigid in its developmental program.

Modelling of dense (4 hour intervals) time-series data provided important insights into the growth dynamics underlying genotypic differences in root architecture, but from a practical standpoint, we wished to know if similar answers could be derived from fewer data points. We conducted two types of sensitivity tests for each trait by progressively removing data from the analysis to generate pseudo time intervals and either: 1. Comparing the differences in modelled trait values for a single genotype (B73, Figure S3-5), or 2. Comparing the differences in statistical test results among B73, Mo17, and the hybrid (Figure S6-8). Our estimates of the B73 total root volume modelling parameters would not have changed significantly if we would have imaged at any interval of 20 hours or less, whereas 4 versus 24 hour intervals gave statistically

211 different results. Model estimates of total branch number hardly varied at pseudo time interval
212 from 4 to 24 hours with a few sporadic exceptions. However, total root length estimates were
213 extremely labile, resulting in significant differences in the values between 4 hours and nearly
214 every other interval (Figure S3-5). Despite this intra-genotypic variability, the computed
215 statistical differences among B73, Mo17, and the hybrid were remarkably consistent at any time
216 interval from 4 to 24 hours for all three traits (Figure S6-8). The results of this analysis suggest
217 that much of the same information about root growth dynamics could be attained through less
218 frequent phenotyping, which could translate to increases in sample throughput, and more power
219 to resolve subtle environmental or genetic differences.

(a) parameters for total root volume

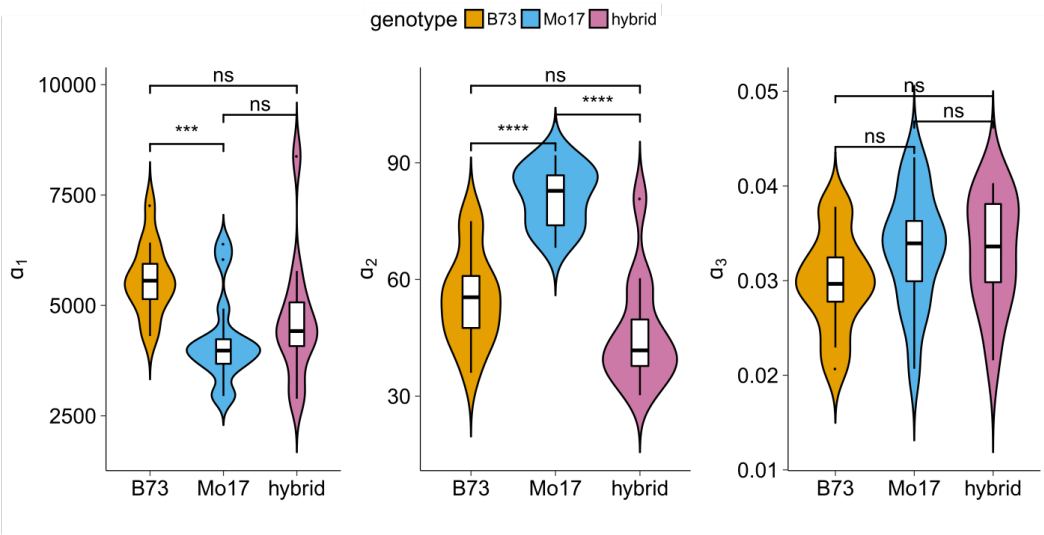

(b) parameters for total root length

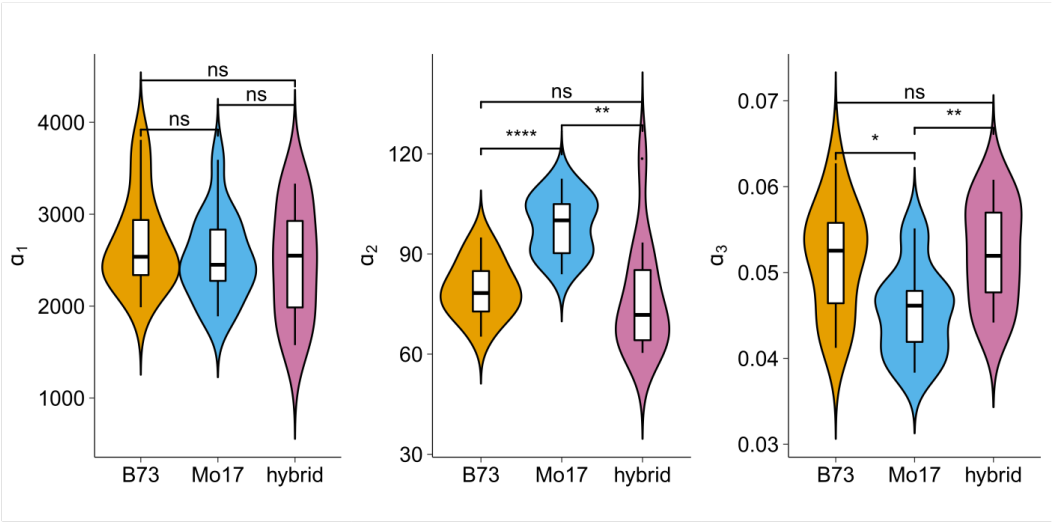

(c) parameters for total number of branches

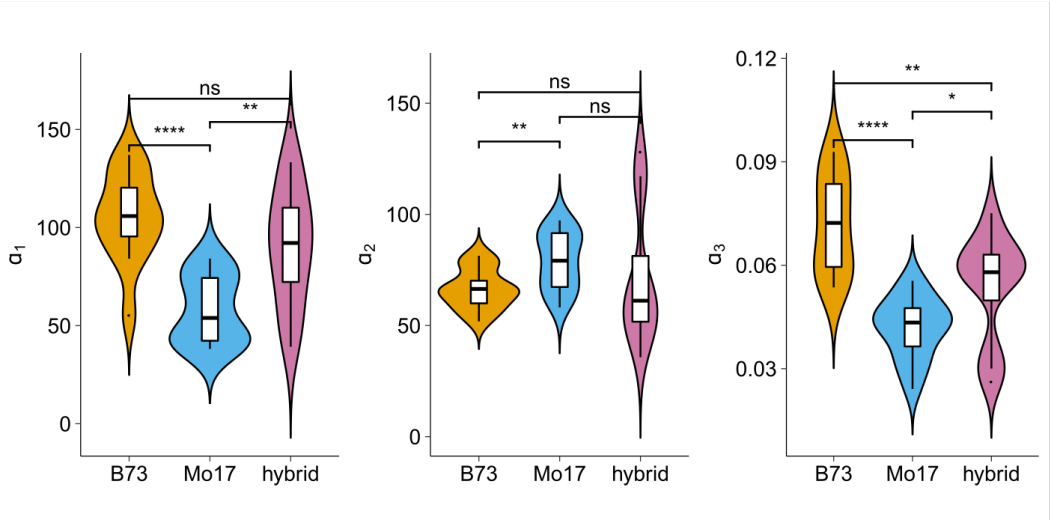

Figure 3. Comparison of global growth patterns by modelling. Parameters (α1, α2, α3) of the logistic growth models estimated for total root volume (a), total root length (b), and total root number (c). Violin plots and box plots were generated using ggplot2 package with default settings for statistics in R. The significance levels of pairwise t tests were added. (ns: p>0.05, *: p<=0.05, **: p<=0.01, ***: p<=0.001, ****: p<=0.0001)

Analysis of the time function reveals local growth patterns driving genotypic differences in root architecture

Root architecture is a global property determined by the cumulative elongation, branching, and curving of each root. Yet much is unknown as to how these local parameters emerge as global root system properties, especially in the context of three dimensional complexity. A key feature of our phenotyping pipeline is automated derivation of the time function and quantification of local growth (Methods). We analyzed all of the individual branches as aggregate trait distributions during the timecourse, from which fundamental differences in growth patterns between genotypes were discerned (Figure 4). Analysis of root length distributions showed that while B73 had a higher proportion of longer branches than Mo17 at the earliest time points, the proportion of shorter branches increased rapidly for B73 during the 5-7 days after germination (DAG) (Figure 4a). This trend reflects the rapid proliferation of lateral roots captured in the global architecture and growth modeling analyses (Figure 2,c,f and 3c). However the burst of new roots quickly tapered by 8DAG as B73 increasingly elongated existing roots, rather than forming new ones. This fundamental shift in resource allocation is clearly seen by the steadily decreasing proportion of relatively shorter roots throughout the rest of the experiment (Figure 4a). In comparison, the architecture of Mo17 was initially defined by shorter roots, but then consistently balanced existing root elongation and new root production throughout the timecourse, reflected in the steady root length distributions seen from 8DAG. Growth patterns of the hybrid were the most consistent, but there was a greater emphasis on new root production relative to Mo17.

To study root curving, we computed the soil angle distribution, which captures root geometry relative to an extrinsic reference (the soil horizon), and branching angle distribution, which measures the intrinsic angle between a child and parent branch regardless of orientation to the soil horizon. As shown in Fig. 4b, B73 had relatively larger soil angles relative to Mo17 at the early time points, indicating that B73 root systems begin growing at a steeper angle. However the proportion of shallow-angled branches quickly increased with the emergence of new branches (Figure 2c), peaking at 7DAG for B73 and the hybrid, but Mo17 was quite consistent during the experiment. Since most roots eventually orient to the vertical gravity vector over time, the production of new lateral roots and their angles relative to the parent branch (which is older and thus more likely to be vertically-oriented) largely dictate the extent of horizontal soil exploration. In the earliest stages of maize root development, several embryonic (seminal) roots emerge from the seed, which is reflected in all three genotypes by the dominance of shallow root

branching angles at the earliest time points. As the root system architecture became more complex over time, branching angle distribution patterns were remarkably consistent, but the magnitudes depended on genotype (Figure 4c). The relatively greater angles for B73 demonstrate that lateral roots grew further away from the parent branch than for Mo17 and the hybrid, highlighting fundamental differences in local growth patterns that have strong implications for root architecture and resource capture (Postma et al., 2014).

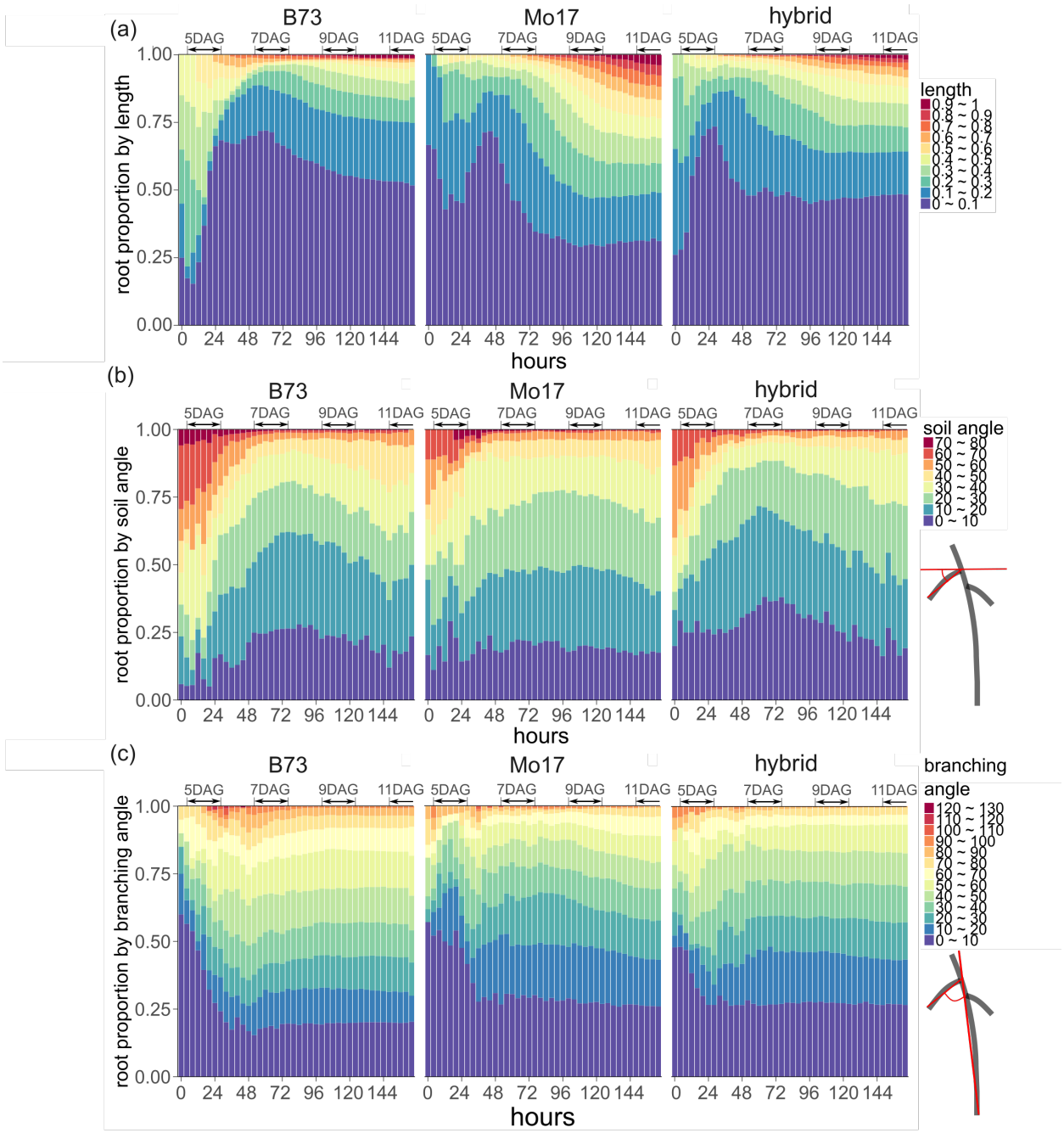

Figure 4. Local growth patterns revealing genotypic differences.

(a) Timecourse of root length distribution. Root length for each individual branch was normalized by the longest branch in the whole root system and recorded in 10 bins. (b) Timecourse of soil angle distribution. The soil angle was the angle formed by the root branch and the horizontal level. (c) Timecourse of branching angle distribution. The branching angle was the angle formed by the child branch and its parent branch.

High-resolution analysis along a single root reveals developmental processes driving genotypic differences in root architecture

Genetic variation for intrinsic developmental processes result in an astonishing diversity of plant morphology. Single roots have been used extensively to study plant development, in part because the position of lateral roots are arranged longitudinally across time, with the youngest organ always nearest to the growing tip at the beginning of the maturation zone (Petricka et al., 2012). To understand how genotypic differences in root development contribute to the emergence of complex architectures, we computed the branch hierarchies for entire root systems, enabling us to know the precise topological relationships of all the roots in each 3D model (Methods). For the final, most architecturally complex time point, we defined the primary root as the branch connected to the seed which had the most child branches, and analyzed the patterns along this developmental axis. The positions of each lateral root were computed using the distance between the branching fork and the base of the primary root, divided by the primary root length (Figure 5a). B73 had more total lateral branches along the primary root than Mo17, but they also emerged much closer to the root tip. On average, B73 lateral roots emerged along the upper 80% of the primary root, whereas Mo17 lateral roots emerged along only the upper 60%. Since there was no significant difference in the primary root length between the two genotypes, B73 had both a higher lateral root branching density and a longer zone of branching. These data are parsimonious with the local and global root length and branching traits we measured previously (Figures 2 and 4). Thus, the basis for the architectural tradeoff of investment in new branches versus growth of existing branches is apparently controlled by genetic differences in local developmental processes.

The radial position of new lateral roots is another developmental attribute that could influence 3D root system properties (Topp and Benfey 2011). Lateral roots develop from pericycle cells adjacent to vascular tissue. The well-studied 2D branching plane of *Arabidopsis thaliana* results from a simple diarch symmetry of vascular strands, but the polyarch symmetry of maize and other monocots promotes the radial emergence of lateral roots (Smith and De Smet, 2012). To quantify if genotype-specific radial emergence patterns contributed to differences in global architecture, we leveraged our 3D data to compute radial angles for lateral branching around the primary root. Each lateral was compared to the adjacent branch along the longitudinal axis, and the relative angle between them was recorded in 10 bins, 36 degrees apart. The mean distributions of the radial angle had a near constant probability, suggesting that lateral roots overall emerged in all directions equally for B73, Mo17, and their hybrid (Figure 5b; mean

values). However, the significant intra-plant variation across the experiment points to substantial heterogeneity along any given primary root, suggesting that radial angle is either stochastic or that micro-environmental conditioning may play a strong role.

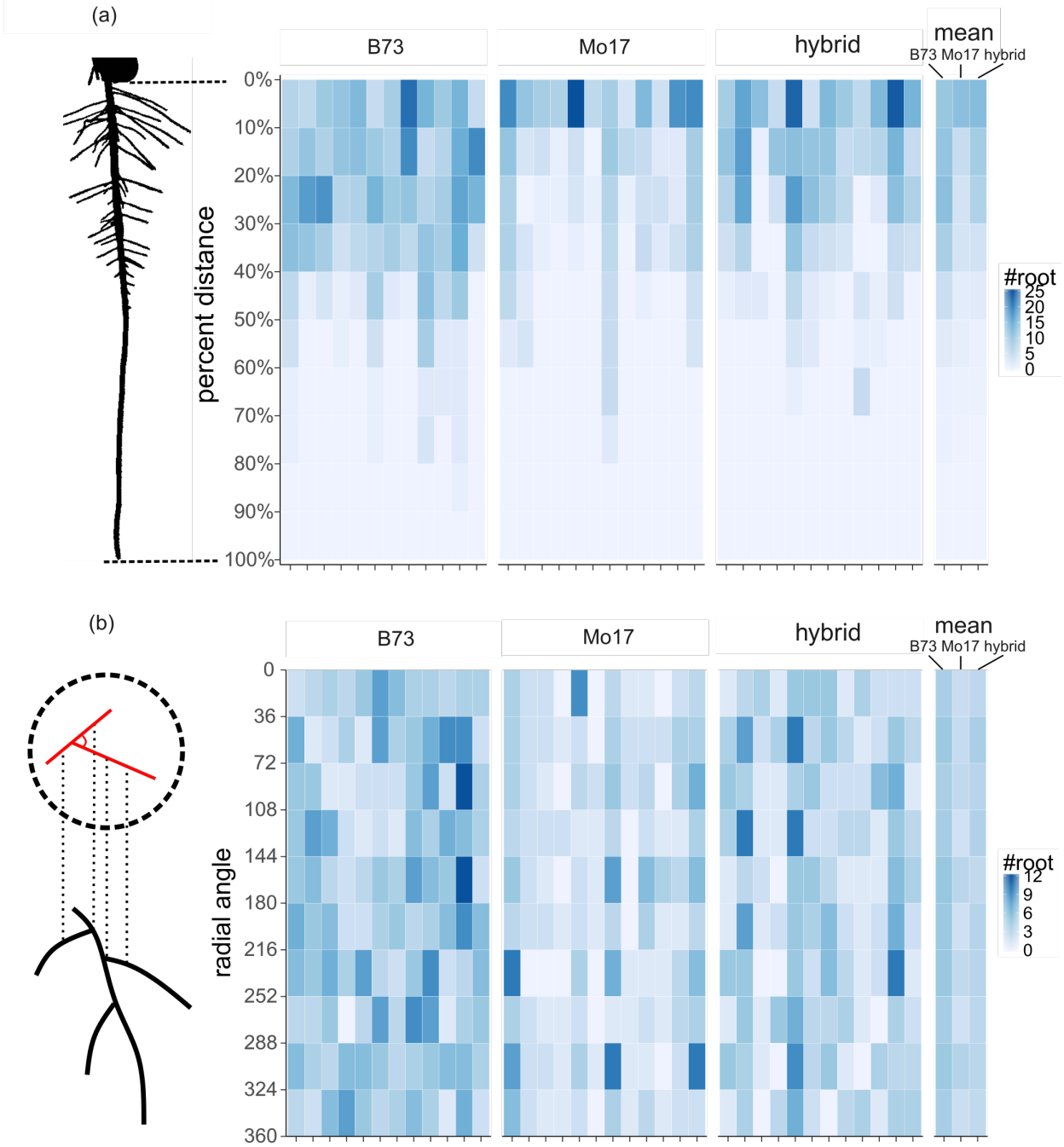

Figure 5. Developmental analysis along primary root revealing genotypic difference. (a) Distribution of the first-order lateral root number on the primary root. The percent distance referred to the distance between the branching fork to the primary root base, divided by the primary root length. (b) Distribution of the radial angles for lateral branching around the primary root. The radial angle was the angle formed by the root branch and the adjacent branch along the longitudinal axis. For each genotype, each column represented an individual seedling.

DISCUSSION

Here we quantified high-resolution spatiotemporal dynamics of maize seedling root systems in three dimensions as they rapidly grew in complexity. Mathematical modelling allowed us to evaluate the contributions of genotype by simple function-values that integrated growth trends in both real and developmental timescales. We demonstrate how differences in aggregate local growth dynamics and developmental characteristics along a single root can condition emergent global architectures, resulting in a highly branched, dense root system for B73 and a more open and extensive system for Mo17. 3D X-ray-based analysis of excavated mature root crowns from two years of field experiments suggested these architectural properties are developmentally and environmentally stable.

When considered in the context of rhizoeconomic foraging strategy (Lynch et al., 2005), the maize inbreds contrast for their carbon investments in new root production relative to maintenance of existing root growth. These differences have significant implications for resource acquisition. Previous studies have posited that the ideotype of fewer but longer lateral roots (Mo17) acquires mobile resources like nitrogen more efficiently, but the ideotype of finer but denser lateral roots (B73) acquires immobile resources like phosphorous more efficiently (Lynch, 2013). Thus our findings extend the known P efficiency of B73 and inefficiency of Mo17 (Kaeppler et al., 2000; Zhu et al., 2005) to include a basis in root growth dynamics. Through "computational dissection" of highly resolved spatiotemporal data, we have shown how genetic differences in complex developmental and local growth patterns measurable at the seedling level can be diagnostic of root architecture at maturity. Similar tradeoffs for thoroughness versus extent of soil exploration have been previously identified in rice seedling root systems, including apparent genetic tradeoffs (Topp et al., 2013). Automated phenotyping and time-resolved analysis applied to mapping populations or association panels would resolve the genetic basis of complex root architecture dynamics, as it has for simpler root traits (Moore et al., 2013b; Kwak et al., 2014). Such function-valued approaches provide fundamentally superior insights into biological growth and environmental interactions than simple summary statistics (Stinchcombe et al., 2012).

With the information of local traits, the contribution of individual branches to the whole root system architecture can be studied. Despite a wide range of phenotypic variation within the root system of a single plant or among genetically identical plants, the overall patterns were strongly correlated with genotype. Considering the homogenous conditions of the gel growth system, we suggest a significant amount of probabilistic behavior is typical to root foraging, which may be modified by local environmental cues or systemic internal processes. Our multiscalar approach can be extended to a wide variety of other studies where local interactions, such as patchy nutrients or competing roots, can be studied in the context of their effects on global systems. 3D imaging and computational analysis of root growth allows measurement of traits (e.g. radial

angle) that are not measurable via 2D phenotyping approaches, especially with very complex root systems. Here we directly compared 3D architectures of seedling and mature root crowns using the same algorithms. Our methods transfer to any 3D data, including the growing body of X-ray tomography and magnetic resonance imaging root studies (Mooney et al., 2012b; Ahmed et al., 2016; van Dusschoten et al., 2016b; Morris et al., 2017). Such high quality inputs should be especially useful to parameterize and constrain multiscale models that incorporate genotypic differences as probability distributions that reflect the inherent stochasticism in plant growth (Lynch et al., 1997; Dupuy et al., 2010; Bodner et al., 2013; Araya et al., 2016; Kalogiros et al., 2016; Zhao et al., 2017; Postma et al., 2017; Passot et al., 2018; Schnepf et al., 2018). The development of simulation models that can account for and accurately predict root growth and root-environment interactions as a function of genotype will be critical for a realistic understanding of integrated plant biology and the enormous potential of root systems for the improvement of agriculture.

METHODS

Plant materials and growth conditions

Two maize inbred genotypes, B73 and Mo17, and their hybrid were used in this study. The seeds were sterilized with 35% hydrogen peroxide for 20 minutes and rinsed four times with RO water. After soaking in RO water for 8 hours at 29 ºC in the dark, the seeds were sterilized again with 35% hydrogen peroxide for 10 minutes and rinsed four times with sterile water. The seeds were placed at 29 ºC in the dark for incubation. After 2 days, seedlings were planted into glass growth cylinders. The growth medium was made following a modified Hoaglands solution (Zurek et al., 2015). The cylinders were put on a shelf overnight for acclimation before moving them into a growth chamber. The growth conditions were set to 28 ºC during the day and 24 ºC at night. The daylight period lasted 16 hours starting at 6 am.

Imaging system

The imaging system was set up in the growth chamber. It consists of a digital camera (Stingray F-504C, Allied Vision Technologies), a turntable (LT360, LinearX), a near infrared LED light (SOBL, Smart Vision Lights), an optical correction tank, and a personal computer. The schematic details of the imaging system can be seen in (Clark et al., 2011). The near infrared LED was used with a longpass camera filter to provide a high contrast silhouette during the day and to avoid affecting plant growth during night. It was turned on 10 seconds before each imaging course, and was turned off immediately after the rotational sequence was taken. For each imaging course, 180 images were taken at 2º increments. A custom program written in LabVIEW was used to control the image acquisition and set up time lapse imaging, which

enabled the imaging system to take rotational image sequences at regular time points automatically. In this study, all the plants were imaged every 4 hours for a week, until day 11 after germination. For each plant, 41 or 42 image sets were captured.

Quantification of RSA traits

We used the RSA-GiA pipeline to generate the 3D reconstructions from 2D rotational images. The pipeline included three main steps: (1) cropping, to remove the above gel parts from the images; (2) thresholding, to convert the images to binary images, which roots are the foreground; (3) reconstruction, to build the 3D models based on visual hull algorithm (Topp et al., 2013). To analyze a time-series of 3D reconstructions, we used DynamicRoots. DynamicRoots is a software tool which is capable of computing structural and dynamic traits for growing roots (Symonova et al., 2015). It aligns all the models in a time-series, decomposes the 3D root system into individual branches, and records the growth process. The primary output of DynamicRoots is a txt file that includes columns for different root traits at every observation time, and rows for data from every branch. To analyze root growth patterns, we developed R functions for computing global root traits, root growth rate, root growth direction, and root distribution from DynamicRoots-generated files (https://github.com/Topp-Roots-Lab/timeseries_analysis). Using the traits for each branch, the total volume, total length, and total number of branches were obtained for every time point. In order to avoid noise, branches shorter than 5 voxels at the last observation time were removed. The total root volume was the sum of the root volume of all individual roots. The total root length was the sum of the root length of all individual roots. The total number of branches was the sum of the numbers of individual roots. The growth rate was the difference of root traits between two subsequent time points. We defined the angle between branch and soil level as soil angle, and the angle between branch and its parent branch as branching angle.

Data analysis

To compare the shape of root growth for different genotypes, we modeled the dynamic of global root traits. Linear, exponential, power law, monomolecular, three-parameter logistic, four-parameter logistic, and Gompertz models were tested. The basic functional forms for these models can be seen in Paine et al., 2012. We parameterized the three-parameter logistic model in the following way to facilitate descriptions of growth curves:

$$y(t) = \frac{\alpha_1}{1 + e^{-\alpha_3(t-\alpha_2)}}$$

where y represents the global traits, i.e. total root volume, total root length, and total root number, t is the time after the start of the imaging course, α_1 is the maximum growth capacity, α_2 is the inflection time point, and α_3 is the steepness.

The parameters for all models were estimated using linear ("lm" function) or non-linear least squares regression ("nls" function) in R. To select the best model, R squared (R^2), root mean

443 squared error (RMSE), standard error (S), and Akaike Information Criterion (AIC) of the
444 regression were computed. t- test was used to compare the parameters among different
445 genotypes.
446
447
448 **Works Cited**

449 **Ahmed, S., Klassen, T.N., Keyes, S., Daly, M., Jones, D.L., Mavrogordato, M., Sinclair, I.,**
450 **and Roose, T.** (2016). Imaging the interaction of roots and phosphate fertiliser granules
451 using 4D X-ray tomography. Plant Soil **401**: 125–134.

452 **Araya, T., Kubo, T., von Wirén, N., and Takahashi, H.** (2016). Statistical modeling of
453 nitrogen-dependent modulation of root system architecture in Arabidopsis thaliana. J.
454 Integr. Plant Biol. **58**: 254–265.

455 **Bao, Y. et al.** (2014). Plant roots use a patterning mechanism to position lateral root branches
456 toward available water. Proc. Natl. Acad. Sci. U. S. A. **111**: 9319–9324.

457 **Barlow, P.W., Brain, P., and Parker, J.S.** (1991). Cellular Growth in Roots of a Gibberellin-
458 Deficient Mutant of Tomato (Lycopersicon esculentum Mill.) and its Wild-type. J. Exp.
459 Bot. **42**: 339–351.

460 **Bodner, G., Leitner, D., Nakhforoosh, A., Sobotik, M., Moder, K., and Kaul, H.-P.** (2013).
461 A statistical approach to root system classification. Front. Plant Sci. **4**: 292.

462 **Borisjuk, L., Rolletschek, H., and Neuberger, T.** (2012). Surveying the plant's world by
463 magnetic resonance imaging. Plant J. **70**: 129–146.

464 **Clark, R.T., MacCurdy, R.B., Jung, J.K., Shaff, J.E., McCouch, S.R., Aneshansley, D.J.,**
465 **and Kochian, L.V.** (2011). Three-dimensional root phenotyping with a novel imaging and
466 software platform. Plant Physiol. **156**: 455–465.

467 **de Dorlodot, S., Forster, B., Pagès, L., Price, A., Tuberosa, R., and Draye, X.** (2007). Root
468 system architecture: opportunities and constraints for genetic improvement of crops. Trends
469 Plant Sci. **12**: 474–481.

470 **Doussan, C., Pagès, L., and Vercambre, G.** (1998). Modelling of the Hydraulic Architecture of
471 Root Systems: An Integrated Approach to Water Absorption—Model Description. Ann.
472 Bot. **81**: 213–223.

473 **Dupuy, L., Gregory, P.J., and Bengough, A.G.** (2010). Root growth models: towards a new
474 generation of continuous approaches. J. Exp. Bot. **61**: 2131–2143.

475 **van Dusschoten, D., Metzner, R., Kochs, J., Postma, J.A., Pflugfelder, D., Bühler, J.,**
476 **Schurr, U., and Jahnke, S.** (2016a). Quantitative 3D Analysis of Plant Roots Growing in
477 Soil Using Magnetic Resonance Imaging. Plant Physiol. **170**: 1176–1188.

van Dusschoten, D., Metzner, R., Kochs, J., Postma, J.A., Pflugfelder, D., Bühler, J., Schurr, U., and Jahnke, S. (2016b). Quantitative 3D Analysis of Plant Roots Growing in Soil Using Magnetic Resonance Imaging. Plant Physiol. **170**: 1176–1188.

Fang, S., Yan, X., and Liao, H. (2009). 3D reconstruction and dynamic modeling of root architecture in situ and its application to crop phosphorus research. Plant J. **60**: 1096–1108.

French, A., Ubeda-Tomás, S., Holman, T.J., Bennett, M.J., and Pridmore, T. (2009). High-throughput quantification of root growth using a novel image-analysis tool. Plant Physiol. **150**: 1784–1795.

Garbout, A., Munkholm, L.J., Hansen, S.B., Petersen, B.M., Munk, O.L., and Pajor, R. (2012). The use of PET/CT scanning technique for 3D visualization and quantification of real-time soil/plant interactions. Plant Soil **352**: 113–127.

Hodge, A., Berta, G., Doussan, C., Merchan, F., and Crespi, M. (2009). Plant root growth, architecture and function. Plant Soil **321**: 153–187.

Hund, A., Reimer, R., Stamp, P., and Walter, A. (2012). Can we improve heterosis for root growth of maize by selecting parental inbred lines with different temperature behaviour? Philos. Trans. R. Soc. Lond. B Biol. Sci. **367**: 1580–1588.

Iijima, M., Oribe, Y., Horibe, Y., and Kono, Y. (1998). Time Lapse Analysis of Root Elongation Rates of Rice and Sorghum During the Day and Night. Ann. Bot. **81**: 603–607.

Iyer-Pascuzzi, A.S., Symonova, O., Mileyko, Y., Hao, Y., Belcher, H., Harer, J., Weitz, J.S., and Benfey, P.N. (2010). Imaging and analysis platform for automatic phenotyping and trait ranking of plant root systems. Plant Physiol. **152**: 1148–1157.

Jahnke, S. et al. (2009). Combined MRI–PET dissects dynamic changes in plant structures and functions. Plant J. **59**: 634–644.

Johnson, M.G., Tingey, D.T., Phillips, D.L., and Storm, M.J. (2001). Advancing fine root research with minirhizotrons. Environ. Exp. Bot. **45**: 263–289.

Kaeppler, S.M., Parke, J.L., Mueller, S.M., Senior, L., Stuber, C., and Tracy, W.F. (2000). Variation among Maize Inbred Lines and Detection of Quantitative Trait Loci for Growth at Low Phosphorus and Responsiveness to Arbuscular Mycorrhizal Fungi Work supported by USDA-Hatch, University of Wisconsin University-Industry Relations, and Cargill Fertilizer. Crop Sci. **40**: 358–364.

Kalogiros, D.I., Adu, M.O., White, P.J., Broadley, M.R., Draye, X., Ptashnyk, M., Bengough, A.G., and Dupuy, L.X. (2016). Analysis of root growth from a phenotyping data set using a density-based model. J. Exp. Bot. **67**: 1045–1058.

Kwak, I.-Y., Moore, C.R., Spalding, E.P., and Broman, K.W. (2014). A simple regression-based method to map quantitative trait loci underlying function-valued phenotypes. Genetics **197**: 1409–1416.

Lambers, H., Shane, M.W., Cramer, M.D., Pearse, S.J., and Veneklaas, E.J. (2006). Root structure and functioning for efficient acquisition of phosphorus: Matching morphological and physiological traits. Ann. Bot. **98**: 693–713.

Lobet, G., Pagès, L., and Draye, X. (2011). A novel image-analysis toolbox enabling quantitative analysis of root system architecture. Plant Physiol. **157**: 29–39.

Lynch, J. (1995). Root Architecture and Plant Productivity. Plant Physiol. **109**: 7–13.

Lynch, J.P. (2013). Steep, cheap and deep: an ideotype to optimize water and N acquisition by maize root systems. Ann. Bot. **112**: 347–357.

Lynch, J.P., Ho, M.D., and Phosphorus, L. (2005). Rhizoeconomics: Carbon costs of phosphorus acquisition. Plant Soil **269**: 45–56.

Lynch, J.P., Nielsen, K.L., Davis, R.D., and Jablokow, A.G. (1997). SimRoot: Modelling and visualization of root systems. Plant Soil **188**: 139–151.

Mairhofer, S., Zappala, S., Tracy, S.R., Sturrock, C., Bennett, M., Mooney, S.J., and Pridmore, T. (2012). RooTrak: automated recovery of three-dimensional plant root architecture in soil from x-ray microcomputed tomography images using visual tracking. Plant Physiol. **158**: 561–569.

Mathews, A.J., Li, K., Wen, J., and Komarov, S. (2014). A dedicated high-resolution PET imager for plant sciences. and biology.

Metzner, R., Eggert, A., van Dusschoten, D., Pflugfelder, D., Gerth, S., Schurr, U., Uhlmann, N., and Jahnke, S. (2015). Direct comparison of MRI and X-ray CT technologies for 3D imaging of root systems in soil: potential and challenges for root trait quantification. Plant Methods **11**: 17.

Miller, N.D., Parks, B.M., and Spalding, E.P. (2007). Computer-vision analysis of seedling responses to light and gravity. Plant J. **52**: 374–381.

Mooney, S.J., Pridmore, T.P., Helliwell, J., and Bennett, M.J. (2012a). Developing X-ray Computed Tomography to non-invasively image 3-D root systems architecture in soil. Plant Soil **352**: 1–22.

Mooney, S.J., Pridmore, T.P., Helliwell, J., and Bennett, M.J. (2012b). Developing X-ray Computed Tomography to non-invasively image 3-D root systems architecture in soil. Plant Soil **352**: 1–22.

Moore, C.R., Johnson, L.S., Kwak, I.-Y., Livny, M., Broman, K.W., and Spalding, E.P. (2013a). High-throughput computer vision introduces the time axis to a quantitative trait map of a plant growth response. Genetics **195**: 1077–1086.

Moore, C.R., Johnson, L.S., Kwak, I.-Y., Livny, M., Broman, K.W., and Spalding, E.P. (2013b). High-throughput computer vision introduces the time axis to a quantitative trait

map of a plant growth response. Genetics **195**: 1077–1086.

Morris, A.K. and Silk, W.K. (1992). USE OF A FLEXIBLE LOGISTIC FUNCTION TO DESCRIBE AXIAL GROWTH OF PLANTS. Bulletin of Mathematical Biology **54**: 1069–1081.

Morris, E.C. et al. (2017). Shaping 3D Root System Architecture. Curr. Biol. **27**: R919–R930.

Muraya, M.M., Chu, J., Zhao, Y., Junker, A., Klukas, C., Reif, J.C., and Altmann, T. (2017). Genetic variation of growth dynamics in maize (Zea mays L.) revealed through automated non-invasive phenotyping. Plant J. **89**: 366–380.

Nagel, K.A. et al. (2012). GROWSCREEN-Rhizo is a novel phenotyping robot enabling simultaneous measurements of root and shoot growth for plants grown in soil-filled rhizotrons. Funct. Plant Biol. **39**: 891–904.

Paine, C.E.T., Marthews, T.R., Vogt, D.R., Purves, D., Rees, M., Hector, A., and Turnbull, L.A. (2012). How to fit nonlinear plant growth models and calculate growth rates: an update for ecologists. Methods Ecol. Evol. **3**: 245–256.

Passot, S., Moreno-Ortega, B., Moukouanga, D., Balsera, C., Guyomarc'h, S., Lucas, M., Lobet, G., Laplaze, L., Muller, B., and Guédon, Y. (2018). A New Phenotyping Pipeline Reveals Three Types of Lateral Roots and a Random Branching Pattern in Two Cereals. Plant Physiology.

Petricka, J.J., Winter, C.M., and Benfey, P.N. (2012). Control of Arabidopsis root development. Annu. Rev. Plant Biol. **63**: 563–590.

Postma, J.A., Dathe, A., and Lynch, J.P. (2014). The optimal lateral root branching density for maize depends on nitrogen and phosphorus availability. Plant Physiol. **166**: 590–602.

Postma, J.A., Kuppe, C., Owen, M.R., Mellor, N., Griffiths, M., Bennett, M.J., Lynch, J.P., and Watt, M. (2017). OpenSimRoot: widening the scope and application of root architectural models. New Phytol. **215**: 1274–1286.

Rellán-Álvarez, R. et al. (2015). GLO-Roots: an imaging platform enabling multidimensional characterization of soil-grown root systems. Elife **4**.

Schnepf, A., Leitner, D., Landl, M., Lobet, G., Mai, T.H., Morandage, S., Sheng, C., Zörner, M., Vanderborght, J., and Vereecken, H. (2018). CRootBox: a structural-functional modelling framework for root systems. Ann. Bot.

Smith, S. and De Smet, I. (2012). Root system architecture: insights from Arabidopsis and cereal crops. Philos. Trans. R. Soc. Lond. B Biol. Sci. **367**: 1441–1452.

Stinchcombe, J.R., Function-valued Traits Working Group, and Kirkpatrick, M. (2012). Genetics and evolution of function-valued traits: understanding environmentally responsive phenotypes. Trends Ecol. Evol. **27**: 637–647.

584 **Symonova, O., Topp, C.N., and Edelsbrunner, H.** (2015). DynamicRoots: A Software
585 Platform for the Reconstruction and Analysis of Growing Plant Roots. PLoS One **10**:
586 e0127657.

587 **Topp, C.N., Benfey P.N.** (2011). Growth Control of Root Architecture. In Plant Biotechnology
588 and Agriculture: Prospects for the 21st Century. Eds. Altman, A. and Hasegawa, P.M.

589 **Topp, C.N. et al.** (2013). 3D phenotyping and quantitative trait locus mapping identify core
590 regions of the rice genome controlling root architecture. Proc. Natl. Acad. Sci. U. S. A. **110**:
591 E1695–704.

592 **Topp, C.N., Bray, A.L., Ellis, N.A., and Liu, Z.** (2016). How can we harness quantitative
593 genetic variation in crop root systems for agricultural improvement? J. Integr. Plant Biol.
594 **58**: 213–225.

595 **Walter, A., Silk, W.K., and Schurr, U.** (2009). Environmental effects on spatial and temporal
596 patterns of leaf and root growth. Annu. Rev. Plant Biol. **60**: 279–304.

597 **Walter, A., Spies, H., Terjung, S., Küsters, R., Kirchgessner, N., and Schurr, U.** (2002).
598 Spatio-temporal dynamics of expansion growth in roots: automatic quantification of diurnal
599 course and temperature response by digital image sequence processing. J. Exp. Bot. **53**:
600 689–698.

601 **Yazdanbakhsh, N. and Fisahn, J.** (2009). High throughput phenotyping of root growth
602 dynamics, lateral root formation, root architecture and root hair development enabled by
603 PlaRoM. Funct. Plant Biol. **36**: 938–946.

604 **Zhang, X. et al.** (2017). High-Throughput Phenotyping and QTL Mapping Reveals the Genetic
605 Architecture of Maize Plant Growth. Plant Physiol. **173**: 1554–1564.

606 **Zhao, J., Bodner, G., Rewald, B., Leitner, D., Nagel, K.A., and Nakhforoosh, A.** (2017).
607 Root architecture simulation improves the inference from seedling root phenotyping
608 towards mature root systems. J. Exp. Bot.

609 **Zhu, J., Kaeppler, S.M., and Lynch, J.P.** (2005). Mapping of QTLs for lateral root branching
610 and length in maize (Zea mays L.) under differential phosphorus supply. Theor. Appl.
611 Genet. **111**: 688–695.

612 **Zurek, P.R., Topp, C.N., and Benfey, P.N.** (2015). Quantitative trait locus mapping reveals
613 regions of the maize genome controlling root system architecture. Plant Physiol. **167**: 1487–
614 1496.

615